Characterization of complex planar faults in FeAl(B) alloys

Bernard Viguier [a, *], Mayerling Martinez [b], Jacques Lacaze [a]

[a] CIRIMAT, Université de Toulouse, INP/ENSIACET, 31030, France
[b] ENSICAEN, Université de Caen, CNRS, 14050 Caen, France

ARTICLE INFO

Keywords:
Intermetallics (aluminides)
Microalloying
Dislocation geometry and arrangement
Electron microscopy
Transmission

ABSTRACT

Complex planar faults were observed by diffraction contrast transmission electron microscopy in a B2 FeAl based alloy containing Ni and B. The comparison of experimental images to simulated ones revealed the detailed structure of these faults that lie on {001} planes with both in-plane and out-of-plane components of the displacement vector. It was deduced that these defects form by segregation of (B-Al vacancies) complexes on a<100> dislocations, leading to various defect structures depending on the screw or edge character of the dislocation.

1. Introduction

Alloys based on the FeAl iron aluminide intermetallic compound have been widely studied over the last three decades [1–4]. Such alloys present good mechanical properties as well as oxidation and corrosion resistance associated with a reasonable cost. However, these alloys suffer from low ductility at room temperature due to grain boundary brittleness and show a decrease in creep resistance at temperatures higher than 600 °C. Efforts to improve their mechanical properties include microalloying, grain size reduction and oxide dispersion strengthening [5]. Crimp and Vedula [6] noticed that adding boron to binary alloys changes the mode of fracture from intergranular to transgranular, thus improving ductility. In addition, they observed that the microstructure of boron doped FeAl alloys shows a considerable amount of planar features when observed by Transmission Electron Microscopy (TEM) [6]. Similar features were further observed in FeAl based alloys directly following the processing [7] of after plastic deformation [8]. The modification of dislocations and antiphase boundary (APB) structures due to the segregation of vacancies was reported in FeAl B2 alloys [9,10]. It was shown that the yield stress anomaly of FeAl compounds could be related to such interactions between vacancies and dislocation [11]. More generally, the structure of APBs in connection with vacancies and/or solute segregation and their role on the mechanical properties have been studied in various ordered intermetallic compounds such as B2 - CuZn [12], $D0_3$ - Fe_3Al [13] and $L1_2$ - Ni_3Al [14,15].

The present study focuses on defects observed in B2 - FeAl alloys, identified as planar defects lying on {001} planes and characterized by a displacement vector of the type $\mathbf{R} = \frac{a}{2}\langle 010\rangle$. Yoshimi et al. [16] first recognised that this type of defect, which they labelled Complex Planar Faults (CPF), is associated with the presence of boron. In the meantime, some debate occurred on the exact nature of these CPF, first considered as stacking faults (SF) [6,8] they were also associated with precipitates [7]. Finally, a detailed analysis of TEM contrast revealed that CPF present both characteristics of SF and APB defects [17]. Additionally Z contrast microscopy showed that the fault is aluminium depleted and it was suggested that CPF are associated with B segregation [17]. This finding was confirmed by field ion microscopy and 3D atom probe analysis [18,19]. It is worth noting that these defects were observed only in B containing FeAl based alloys with various compositions: Fe-35 at.% Al-0.5 at.%B [16], Fe-35 at.%Al-100 ppm.B [20], Fe-40 at.%Al-0.7 at.% C-0.5 at.%B [21] Fe-40 at.%Al-3.8 at.%Ni-150 ppm.B [19] and Fe-40 at.%Al-2.7 at.%Ni-150 ppm.B (present study and [20]). To summarize the characterization of the CPF as it is now stated, one can describe them as planar faults lying on {001} planes of the B2 structure and presenting both characteristics of SF and APB. The associated displacement vector of the fault is of the type $\mathbf{R} = \frac{a}{2}\langle 010\rangle$ lying in the plane of the defect, though it has been

* Corresponding author.
E-mail address: bernard.viguier@ensiacet.fr (B. Viguier).

http://dx.doi.org/10.1016/j.intermet.2016.12.005

argued that this vector must present some out of plane component [21]. The purpose of the present paper is to characterise CPF in FeAl based B2 compounds more precisely, using conventional diffraction contrast in TEM. The comparison of experimental images to computer-simulated images has allowed us to test various configurations and to quantify the actual components of the displacement vector of the defect. The final objective of this study is to propose a structural model for the CPF and to gain some insight into the comprehension of their formation mechanisms.

2. Material and methods

The FeAl alloy used in this study, was kindly provided to us by Anna Fraczkiewicz from The School of Mines, Saint Etienne, France. The alloy was obtained by fusion under controlled atmosphere (argon) from purified electrolytic iron (C < 10 ppm, S < 10 ppm, O < 10 ppm, N < 10 ppm), aluminium of 99.99% purity and nickel of 99.99% purity. The alloy was homogenised by six successive meltings, during which pure boron was added to the melt, and finally cast in the form of a small rectangular ingot. The alloy was studied as cast and presents a single phase B2 structure with quite large grains (grain size of approximately 1 mm). The chemical composition was measured by inductively coupled plasma – mass spectroscopy analysis that gives (in at %): Fe-56.9, Al-40.6, Ni-2.7 and 150 ppm B. The alloy will be labelled FeAlNiB throughout this paper.

Samples for TEM observations were prepared by mechanical polishing until reaching a 150 μm thick foil approximately and then electropolished by the twin jet method in a Tenupol 5 with an electrolyte consisting of 30% nitric acid and 70% methanol, at −15 °C and 10 V. The TEM characterization of the defects was made in conventional diffraction contrast using a transmission electron microscope JEOL 2010 operating at 200 kV and a double tilt specimen holder. The orientation of the selected grains was determined by searching for three low index zone axes in diffraction mode and plotting them onto a stereographic projection. This was necessary to avoid any ambiguity in the determination of geometrical and structural parameters needed for TEM image simulations. Several images of the same defect were then taken using a wide range of diffraction vectors ($\mathbf{g}$) in bright field mode and close to the Bragg condition. The conventional bright field TEM images obtained in this work were compared to image simulations that were calculated using the multi beam image simulation program Cufour from Schäublin and Stadelmann [22]. The generic data used for the simulation presented in Figs. 3–5 are given in Table 1. The specific data such as geometry and defect configuration is detailed in the results section. The deviation from the exact Bragg condition was determined for each image from the selected area diffraction pattern and is given (in terms of excitation error amplitude $\mathbf{s_g}$) in the corresponding image captions.

3. Results and discussion

3.1. Observation of CPF using conventional TEM

TEM observations of the FeAlNiB alloy in the as-cast state indicate a high density of dislocations and the presence of planar faults, as visible in the general view from Fig. 1. Two types of dislocations are currently observed from the B2 structure of the alloy, namely rectilinear edge dislocations with $\mathbf{b} = a\langle 100\rangle$ and tangled superdislocations with $\mathbf{b} = a\langle 111\rangle$. Several planar defects corresponding to the CPF as described above are visible in this field. They correspond either to isolated extended planar faults marked with a white cross, or to more complex arrangements of faulted bows as indicated by black arrows in Fig. 1. The distribution of dislocations and CPF appears somehow uneven.

One CPF was selected in another area for a more precise analysis of the contrast in order to determine its configuration. The characterization was made by tilting experiments and using different diffracting vectors in two-beam bright field images in the TEM as showed in Fig. 2. Stereographic analysis of the defect shows that it lies on (010) plane and that the bounding dislocations are aligned along $\mathbf{u} = [100]$ direction. The visibility of the defect was analysed depending on the diffraction vector. The defect is completely invisible using $\mathbf{g} = 100$. The defect is fully visible with a 001 diffraction vector, while only the bounding dislocations show contrast with 002. In the same picture, Fig. 2b, one can also notice that both bounding dislocations present the same contrast with black and white lobes on the same side of the dislocation line at the foil emergence, as indicated with white circles. This shows that the two dislocations are of the same sign and do not constitute a dislocation dipole. Since the contrast of both dislocations is very similar, they may have the same Burgers vector. These images, and other bright field and dark field images not shown here, demonstrate that the defect corresponds to two edge partial dislocations with Burgers vector parallel to [001]. The planar fault itself exhibits features of both APB type contrast, or π type contrast, when imaged with superlattice 001 diffraction vector and SF type contrast, or α type, when imaged with fundamental $10\bar{1}$ vector. Thus, this defect actually corresponds to the CPF as proposed earlier by Yoshimi et al. [16] and Pang at al [17].

Based on this classical contrast analysis, the displacement vector of the fault, $\mathbf{R}$, which is connected to the Burgers vector of bounding dislocations, should be $\mathbf{R} = \frac{a}{2}[001]$. However this conclusion is contradicted by the experimental image with $\bar{1}10$ diffraction vector (Fig. 2e) which shows a clear contrast for the fault despite the fact that this diffraction vector should lead to $\alpha = 2\cdot\pi\cdot\mathbf{g}\cdot\mathbf{R} = 0$. Some significant residual contrast is also visible arising from the dislocation lines. This may be explained by the fact that even if $\mathbf{g}\cdot\mathbf{b} = 0$, the secondary condition for the full extinction ($\mathbf{g}\cdot\mathbf{b}\wedge\mathbf{u} = 0$) is not fulfilled. Nevertheless such dislocation residual contrast would be limited to the vicinity of the dislocation line and could not explain the extended fault contrast as observed in Fig. 2e. In 1986, Baker and Gaydosh [7] initially noticed a similar strong residual contrast of CPF under diffraction conditions for which $\alpha = 0$. This was ascribed to a precipitation-like defect. Similar residual contrast was also clearly visible in various images from other studies [8,17]. However, this contrast was not explained and the displacement vector of the fault $\mathbf{R}$ was considered to lie in the fault plane.

The usual analysis of experimental TEM images obtained under conventional or even weak-beam diffraction contrast mode is often not sufficient to quantify the observed defects. Previous studies demonstrated that image simulations may be necessary in many cases, e.g. for accurate measurement of dissociation width [24], analysis of special contrast effects [25] or even the clear identification of dislocation configuration [26]. In order to clarify the origin of the observed contrast, experimental images of CPF were

Table 1
Input parameters used in simulations.

Elastic constants [23]: $C_{11} = 181.1$; $C_{12} = 113.7$; $C_{44} = 127.1$ GPa
Beams used for calculation: $-\mathbf{g}$, 0, $+\mathbf{g}$, $+\mathbf{2g}$
(except for the image with $\mathbf{g} = 010$ for which a strict two beam calculation - 0, $+\mathbf{g}$ - was used)

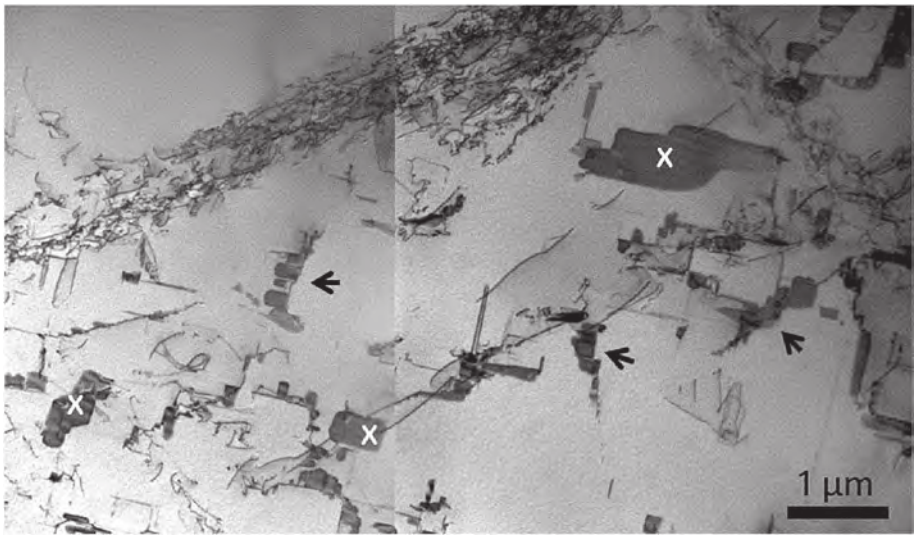

Fig. 1. General view of the defects' structure in a B containing FeAlNi alloy as observed in TEM bright field image. Two structures of planar defects, extended isolated faults and complex arrangements of faulted bows are indicated by white crosses and black arrows respectively.

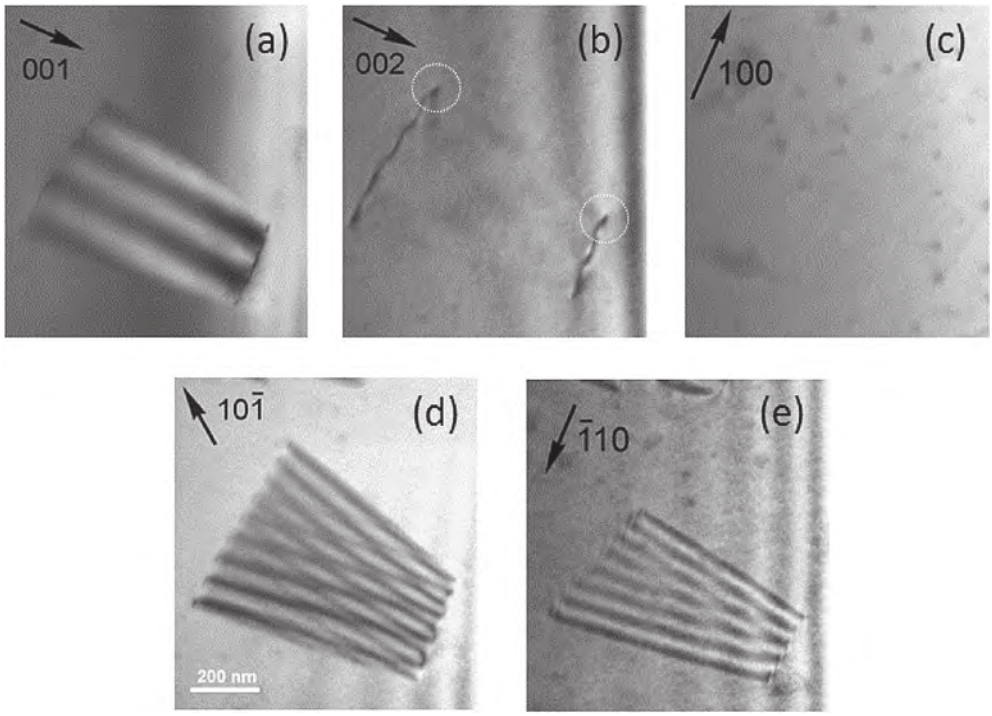

Fig. 2. Bright-field images of a planar fault in a FeAlNiB alloy corresponding to various diffraction vectors.

compared to simulated images calculated with various defect models.

3.2. Image simulation of CPF, comparison with observations

In order to compare the experimental images to simulated ones, the defect presented in Fig. 3 was selected in a region of the thin foil with nearly constant thickness. Fig. 3 shows both experimental and simulated images together with a schematic of the defect. The stereographic analysis indicates that the foil normal is close to [104] and its thickness is 240 nm. The defect lies on (100) plane, the dislocation line **u** is parallel to [001] and the dislocation separation is 460 nm. Classical diffraction contrast analysis similar to the one presented in the previous paragraph indicates that the defect is bordered by partial dislocations possessing the same Burgers vector, $\mathbf{b}_1 = \mathbf{b}_2 = \mathbf{b}$ with edge character. The planar defect was thus characterized by a displacement vector close to $\mathbf{R} = \mathbf{b} = \frac{a}{2}[010]$. The simulation program CUFOUR was run using material data given in Table 1, the geometrical features and various defect vectors are detailed below.

Fig. 3 compares the contrast of the defect under super-lattice 010 and fundamental 020 diffraction vectors as presented on experimental — Fig. 3b and d - and simulated — Fig. 3c and e — images. The defect clearly exhibits a π type contrast since the defect

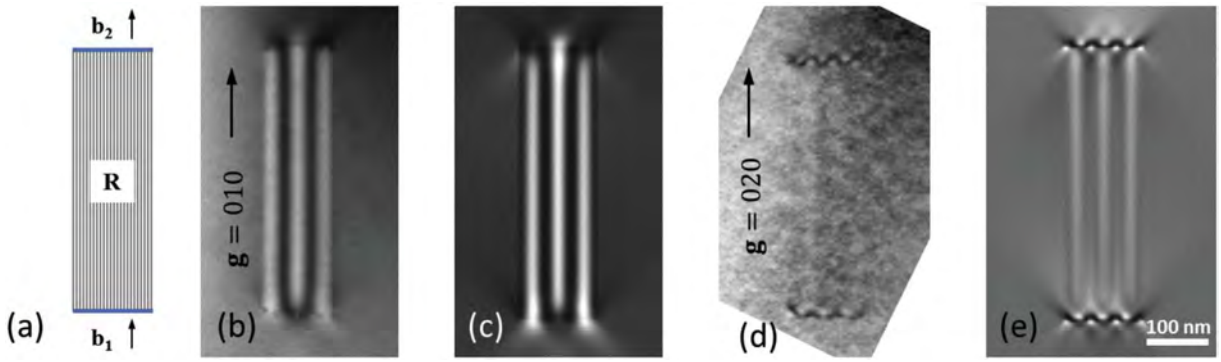

Fig. 3. Schematic (a), experimental (b, d) and simulated (c, e) images of a CPF observed in BF using superlattice 010 ($\mathbf{s_g} = 8.8\ 10^{-4}\ nm^{-1}$) and fundamental 020 ($\mathbf{s_g} = 5.9\ 10^{-3}\ nm^{-1}$) diffraction vectors. The beam direction is $\mathbf{B} = [406]$. See the text for contrast analysis.

is visible with super-lattice reflexion 010 and is barely visible with the fundamental reflexion 020. The simulated images presented in Fig. 3 show that it is possible to reproduce the features of both experimental images nicely. Namely, when imaged with super-lattice 010 vector, the fault contrast is quite strong and the black and white fringes cover the partial dislocation contrast, whereas for diffraction vector 020 the fault is nearly invisible and the dislocation lines exhibit an oscillating black and white lobe contrast, representative of dislocation line contrast with $\alpha = 1$. In accordance to the actual structure of the defect as determined below, simulated images shown in Fig. 3c and e were calculated using an out-of-plane component $\delta = 0.134$. It was verified that introducing such an out-of-plane component δ in the displacement vector does not affect the image contrast in Fig. 3 with $\mathbf{g}//010$.

As mentioned earlier, it has already been observed that CPF in FeAl show quite a strong "residual" contrast when imaged with diffraction vector corresponding to $\alpha = 2\cdot\pi\cdot\mathbf{g}\cdot\mathbf{R} = 0$. For the present CPF defect such residual contrast appears for the diffraction vector $\mathbf{g} = 10\bar{1}$. The corresponding experimental image is shown in Fig. 4a in which one can indeed notice a significant contrast despite $\alpha = 0$. In order to reproduce this contrast, simulations were performed using a displacement vector with an out of plane component in the form of $\mathbf{R} = a\left[\delta\frac{1}{2}0\right]$. It must be noted that introducing this out of plane component δ necessarily leads to distinguishing the Burgers vector of the two bounding dislocations and one may write $\mathbf{b}_1 = a\left[\delta\frac{1}{2}0\right]$ and $\mathbf{b}_2 = a\left[\bar{\delta}\frac{1}{2}0\right]$ so that the sum remains equal to a perfect dislocation of the B2 structure, namely $\mathbf{b}_1 + \mathbf{b}_2 = a[010]$.

Searching for a more quantitative estimation of this out of plane component of the defect vector, a comparison of experimental images with a series of simulation with varying δ values was performed. Firstly, a series of simulations with increasing values of δ by steps of 0.1 was performed. The best agreement was found to correspond to a value of δ between 0.1 and 0.2, and it was then decided to use the value of 0.13 as suggested by Lu et al. for B doped RuAl alloy [27]. A second series of simulations was then performed, setting the out-of-plane value of the defect to 0, 0.13 and 0.27 successively; these simulations are shown in Figs. 4 and 5. The first simulation in Fig. 4b corresponds to $\delta = 0$ where one can see residual contrast from the dislocations solely, as to be expected since the invisibility criterion $\mathbf{g}.\mathbf{b}\wedge\mathbf{u} = 0$ does not hold. However, this residual contrast is strictly limited to the dislocation line and cannot explain the plane defect contrast observed experimentally. The best agreement between experimental and simulated images was obtained for a value of the out of plane component of $\delta = 0.13$, Fig. 4c. The simulated image for a component twice as large

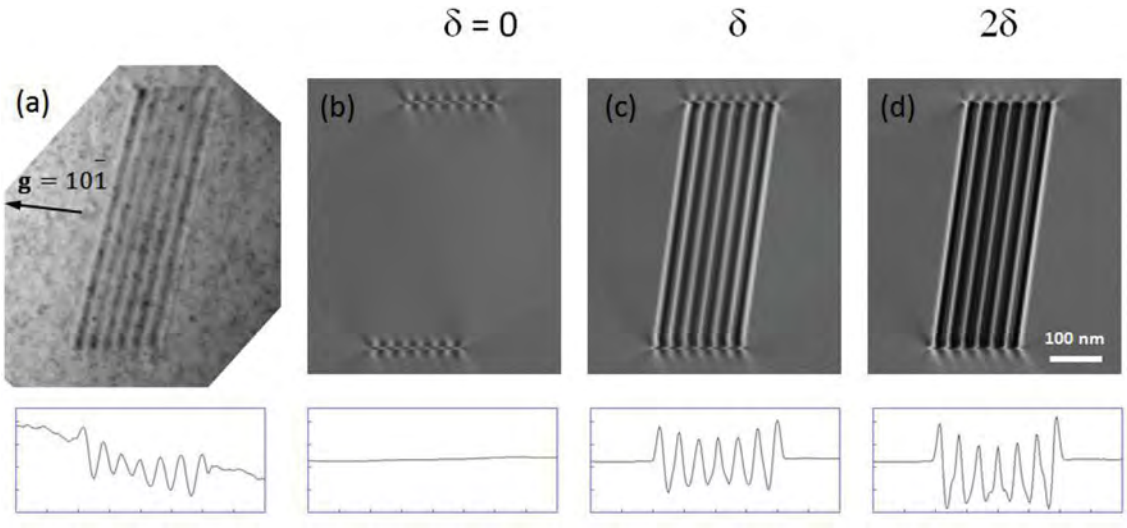

Fig. 4. Comparison of an experimental image (a) of CPF with simulated images (b to d) corresponding to various values of out of plane fault vector component for the 'residual' contrast condition; $\mathbf{g} = 10\bar{1}$, $\mathbf{s_g} = 4.7\ 10^{-3}\ nm^{-1}$ and $\mathbf{B} = [515]$. The intensity profile, measured perpendicularly to the fault fringes, is plotted below each image,.

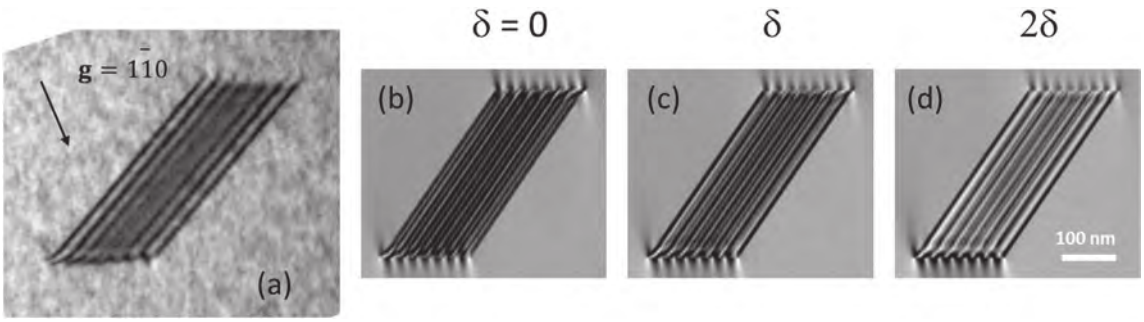

Fig. 5. Comparison of an experimental image (a) of the same CPF as in Figs. 3 and 4 with simulated images (b to d) corresponding to various values of out of plane fault vector component. $\mathbf{g} = 1\bar{1}0$, $\mathbf{s_g} = 2.7\ 10^{-3}\ \mathrm{nm}^{-1}$ and $\mathbf{B} = [334]$.

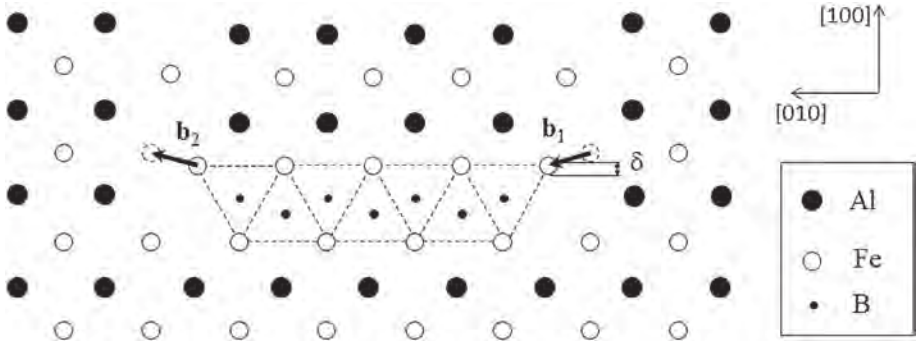

Fig. 6. Schematic of the CPF structure arising from the dissociation of an edge dislocation with $\mathbf{b} = a[010]$ and the segregation of B atoms on (100) plane substituting the Al atoms.

(2δ = 0.27) is shown for comparison, Fig. 4d. The agreement is even more clearly visible when comparing the experimental and calculated intensity profiles (bottom row in Fig. 4). Indeed the simulated image with δ = 0 shows no fringes, the one with δ = 0.13 presents oscillating contrast very similar to the one measured in the experimental image (except for the decreasing base line contrast in the experimental image which can be connected to a wedge shape of the thin foil whilst the simulation was performed, assuming the foil has parallel surfaces), and finally the simulated image with 2δ exhibits some kind of double wave that is not visible in the experimental image.

A similar comparison between experimental and simulated images was also performed for the diffraction vector $\mathbf{g} = 1\bar{1}0$ and is shown in Fig. 5. In this case, both in plane and out of plane components of the defect vector have an incidence on the image contrast through the $\alpha = 2\cdot\pi\cdot\mathbf{g}\cdot\mathbf{R}$ value. The effect of varying δ is thus intermediate between what can be observed with $\mathbf{g} = 010$ (Fig. 3) and $\mathbf{g} = 10\bar{1}$(Fig. 4). Again, a better agreement between experimental and simulated images is observed for δ = 0.13.

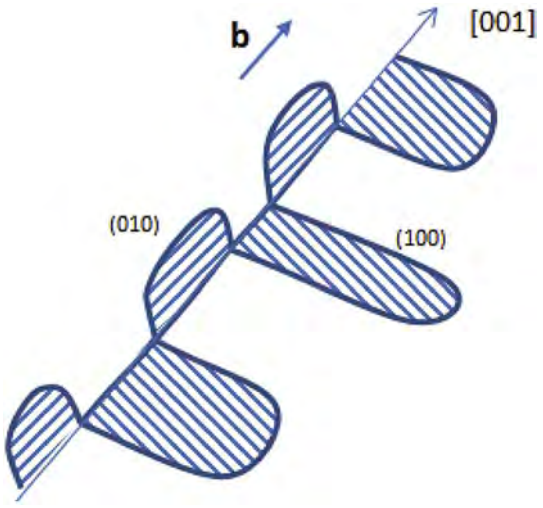

Fig. 7. Schematic of the CPF structure arising from the dissociation of a screw dislocation with $\mathbf{b} = a[001]$ and the segregation of B atoms substituting the Al atoms on (100) and (010) planes.

3.3. CPF structure and discussion

The present work clarifies the structure of CPF currently observed in B containing FeAl based alloys more precisely. The contrast analysis supported by TEM image simulation allowed us to show that the fault displacement possesses both an in-plane (a/2 [010]) and an out of plane (a[δ00]) component with δ = 0.13. Lu et al. [27] conducted similar observations of CPF on B containing RuAl intermetallic with the same B2 structure. These authors show images of CPF observed by conventional diffraction contrast in TEM that present the same characteristics as those presently observed in FeAl compounds. Lu et al. suggested that the defect corresponds to the segregation of B atoms substituting Al atoms on {100} planes of the B2 structure, and further proposed that the CPF consists of a single layer of B_2Ru boride with Ru and B atoms forming trigonal prisms. This structure can be readily adapted to the present case with the dissociation of a dislocation with $\mathbf{b} = a[010]$ as shown in Fig. 6. As demonstrated by Lu et al., the substitution of Al by B leads to a contraction of the planar distance normal to the fault plane. Considering that the prism is based on an equilateral triangle, this contraction can be estimated as a fraction of the B2 lattice parameter, $\delta = 1 - \frac{\sqrt{3}}{2} \approx 0.134$, which is the best value found for the out of plane component in the simulations presented above.

A similar contraction of the same magnitude was also reported by Pang et al. following a Z contrast TEM lattice image [21]. CPF observed in FeAl alloys may thus result from such segregation of B atoms on {100} planes in which B atoms substitute Al atoms. As proposed by Cadel et al. [19] this mechanism is probably driven by the coalescence of coupled B atoms and Al vacancies. In this view it is worth noting that such defects are commonly observed in off-stoichiometry Al lean alloys, i.e. in alloys prone to containing a large amount of Al vacancies. The structure of the CPF as quantified in the present study seems to confirm the fact that two B atoms substitute one Al atom in the default plane thus leading to a one-layer thick B_2Fe boride. Atomic scale calculations of the (B − Al vacancy) complexes on the one hand and of the structure of FeB_2 layers on the other hand would help to elucidate this issue.

All the CPF that we have observed in our study were associated to the dissociation of a<001> dislocations. The dissociation of an edge segment occurs in the glide plane of the dislocation, leading to CPF of simple shape extended in a single plane such as the ones observed in Figs. 2 and 3 or the ones marked with a cross in Fig. 1. Similarly, the edge dislocation can step over two different {100} planes and dissociate in CPF ribbons such as the ones described by Pand and Kumar, (see Fig. 4 in Ref. [21]). If the segregation occurs on a screw dislocation segment, the dissociation can take place on the two {100} planes containing **b** and **u** by the bowing out of a partial dislocation $\frac{a}{2}\langle 001\rangle$. This dissociation mechanism would lead to a defect configuration schematically shown in Fig. 7. This kind of configuration produces structures that are quite complex and commonly observed in B containing FeAl alloys, similar to the ones indicated by black arrows in Fig. 1.

4. Conclusions

The planar defects in boron-containing FeAl alloys have been characterized by combining conventional diffraction contrast in a TEM with computer generated image simulations. These complex planar faults lie in {100} type planes and have a displacement vector with an out of plane component $R = a\left[\delta\,\frac{1}{2}\,0\right]$, with $\delta = 0.134$. This structure was described as a segregation of B atoms that substitute Al atoms based on the segregation of (B − Al vacancy) complexes on a<010> dislocations. This segregation and further dissociation of edge and screw dislocations explain the various CPF structures currently observed in B containing Al lean FeAl alloys.

References

[1] U. Prakash, R.A. Buckley, H. Jones, C.M. Sellars, ISIJ Int. 31 (1991) 1113–1126.
[2] K. Yoshimi, S. Hanada, M.H. Yoo, Intermetallics 4 (1996) S159–S169.
[3] E.P. George, I. Baker, Intermetallics 6 (1998) 759–763.
[4] D.G. Morris, M.A. Muñoz-Morris, Intermetallics 18 (2010) 1279–1284.
[5] D.G. Morris, I. Gutierrez-Urrutia, M.A. Muñoz-Morris, Int. J. Plast. 24 (2008) 1205–1223.
[6] M.A. Crimp, K. Vedula, Mater. Sci. Eng. A 78 (1986) 193–200.
[7] I. Baker, D.J. Gaydosh, Phys. Status Solidi A 96 (1986) 185–190.
[8] Z.Y. Song, H. Hashimoto, C.T. Chou, H. Endoh, Phil. Mag. A 64 (1991) 333–339.
[9] N. Junqua, J.C. Desoyer, P. Moine, Phys. Stat. Sol. A 18 (1973) 387–395.
[10] M.A. Morris, O. George, D.G. Morris, Mater. Sci. Eng. A 258 (1998) 99–107.
[11] D.G. Morris, C.T. Liu, E.P. George, Intermetallics 7 (1999) 1059–1068.
[12] P. Beauchamp, G. Dirras, Phil. Mag. A 67 (1993) 813–826.
[13] J.F. Perez, D.G. Morris, Phil. Mag. A 74 (1996) 665–684.
[14] A. Lasalmonie, B. Chenal, G. Hug, P. Beauchamp, Phil. Mag. A 58 (1988) 543–554.
[15] J.F. Perez, P. Shang, D.G. Morris, I.P. Jones, Phil. Mag. A 79 (1999) 179–192.
[16] K. Yoshimi, S. Hanada, T. Onuma, M.H. Yoo, Phil. Mag. A 73 (1996) 443–456.
[17] L. Pang, M.F. Chisholm, K.S. Kumar, Phil. Mag. Lett. 78 (1998) 349–355.
[18] E. Cadel, D. Lemarchand, A.S. Gay, A. Fraczkiewicz, D. Blavette, Scr. Mater. 41 (1999) 421–426.
[19] E. Cadel, A. Fraczkiewicz, D. Blavette, Scr. Mater 51 (2004) 437–441.
[20] M. Martinez Celis, PhD thesis, Institut National Polytechnique de Toulouse, France (2007) *http://www.theses.fr/2007INPT004G*.
[21] L. Pang, K.S. Kumar, Acta Mater. 49 (2001) 2215–2226.
[22] R. Schäublin, P. Stadelman, Mater. Sci. Eng. A 164 (1993) 373–378.
[23] G. Simmons, H. Wang, Single Crystal Elastic Constants and Calculated Aggregated Properties, MIT Press, Cambridge, 1971.
[24] N. Baluc, R. Schäublin, Philos. Mag. A 74 (1) (1996) 113–136.
[25] B. Viguier, K.J. Hemker, G. Vanderschaeve, Philos. Mag. A 69 (1) (1994) 19–32.
[26] S.M.H. Haghighat, R. Schäublin, J. Nucl. Mater. (2015) 648–652.
[27] D.C. Lu, M. De Graef, T.M. Pollock, Philos. Mag. 84 (2004) 2317–2329.